AMERICAN SOCIETY FOR MICROBIOLOGY | Antimicrobial Agents and Chemotherapy®

ANTIVIRAL AGENTS

Kinetic Characterization and Inhibitor Screening for the Proteases Leading to Identification of Drugs against SARS-CoV-2

Chih-Jung Kuo,[a] Tai-Ling Chao,[b] Han-Chieh Kao,[b] Ya-Min Tsai,[b] Yi-Kai Liu,[a] Lily Hui-Ching Wang,[c] Ming-Chang Hsieh,[d,e] Sui-Yuan Chang,[b,f] Po-Huang Liang[g,h]

[a]Department of Veterinary Medicine, National Chung Hsing University, Taichung, Taiwan
[b]Department of Clinical Laboratory Sciences and Medical Biotechnology, National Taiwan University, Taipei, Taiwan
[c]Institute of Molecular and Cellular Biology, National Tsing Hua University, Hsinchu, Taiwan
[d]Clinical Laboratory, Chung Shan Medical University Hospital, Taichung, Taiwan
[e]Department of Medical Laboratory and Biotechnology, Chung Shan Medical University, Taichung, Taiwan
[f]Department of Laboratory Medicine, National Taiwan University Hospital, Taipei, Taiwan
[g]Institute of Biological Chemistry, Academia Sinica, Taipei, Taiwan
[h]Institute of Biochemical Sciences, National Taiwan University, Taipei, Taiwan

ABSTRACT Coronavirus (CoV) disease 2019 (COVID-19), caused by the severe acute respiratory syndrome coronavirus 2 (SARS-CoV-2), has claimed many lives worldwide and is still spreading since December 2019. The 3C-like protease ($3CL^{pro}$) and papain-like protease (PL^{pro}) are essential for maturation of viral polyproteins in SARS-CoV-2 life cycle and thus regarded as key drug targets for the disease. In this study, $3CL^{pro}$ and PL^{pro} assay platforms were established, and their substrate specificities were characterized. The assays were used to screen collections of 1,068 and 2,701 FDA-approved drugs. After excluding the externally used drugs which are too toxic, we totally identified 12 drugs as $3CL^{pro}$ inhibitors and 36 drugs as PL^{pro} inhibitors active at 10 μM. Among these inhibitors, six drugs were found to suppress SARS-CoV-2 with the half-maximal effective concentration (EC_{50}) below or close to 10 μM. This study enhances our understanding on the proteases and provides FDA-approved drugs for prevention and/or treatment of COVID-19.

KEYWORDS COVID-19, SARS-CoV-2, $3CL^{pro}$, PL^{pro}, inhibitors, antivirals, drug repurposing

The ongoing coronavirus (CoV) disease 2019 (COVID-19) has claimed many lives worldwide since the cases reported in December 2019 (1, 2). The pathogen of COVID-19 is homologous to the severe acute respiratory syndrome (SARS)-associated CoV (SARS-CoV) that caused an outbreak in 2002 to 2003 (3, 4) and was thus named SARS-CoV-2 by WHO. In between, another outbreak of CoV disease that started from the Middle East countries in 2012 and spread to South Korea in 2015 was also caused by a human CoV named Middle East respiratory syndrome CoV (MERS-CoV) (5, 6). The common syndrome of these CoV diseases is an atypical pneumonial infection featured by nonproductive cough, high fever, and headache that may progress to generalized interstitial infiltrates in the lung. For drug repurposing against COVID-19, several approved antivirals which had been previously shown to inhibit SARS-CoV and MERS-CoV were top choices of testing on SARS-CoV-2. For example, favipiravir, ribavirin, and penciclovir which are nucleotide analogues inhibiting viral RNA polymerases (7), as well as the human immunodeficiency virus type 1 (HIV-1) protease inhibitors lopinavir/ritonavir which have been shown to inhibit SARS-CoV and MERS-CoV (8, 9) were earlier investigated but showed weak inhibition of SARS-CoV-2 replication (10, 11). Drugs such as chloroquine, an antimalarial drug that could block virus infection by

Citation Kuo C-J, Chao T-L, Kao H-C, Tsai Y-M, Liu Y-K, Wang LH-C, Hsieh M-C, Chang S-Y, Liang P-H. 2021. Kinetic characterization and inhibitor screening for the proteases leading to identification of drugs against SARS-CoV-2. Antimicrob Agents Chemother 65:e02577-20. https://doi.org/10.1128/AAC.02577-20.

Address correspondence to Sui-Yuan Chang, sychang@ntu.edu.tw, or Po-Huang Liang, phliang@gate.sinica.edu.tw.

Received 11 December 2020
Returned for modification 30 December 2020
Accepted 13 January 2021
Accepted manuscript posted online 1 February 2021
Published 18 March 2021

increasing endosomal pH required for membrane fusion between the virus and the host cell (12), ivermectin, approved as an antiparasitic agent (13) but also has antiviral activity against a broad range of viruses (14), and arbidol, an entry inhibitor against influenza viruses and arboviruses (15), showed relatively lower half-maximal effective concentrations (EC_{50}s) of 1.13, 2.5, and 4.11 μM, respectively, against SARS-CoV-2 *in vitro* (10, 16, 17). However, chloroquine was shown to have no inhibitory effects on SARS-CoV-2 in human lung cells by *in vitro* assay (18). Although hydroxychloroquine, a less toxic derivative of chloroquine, was shown to inhibit SARS-CoV-2 *in vitro* (19), it showed no clinical benefit against COVID-19 (20).

Targeting enzymes essential for viral replication and life cycle of SARS-CoV-2 is a promising strategy. The main protease, also called 3C-like protease ($3CL^{pro}$), and the papain-like protease (PL^{pro}), which cleave 11 and 3 sites on the two polyproteins generated by SARS-CoV inside host cells to yield a total of 16 mature nonstructural proteins (NSPs), are essential for virus replication (21). To execute their functions, $3CL^{pro}$ (NSP5) and PL^{pro} (NSP3) first undergo autocleavage for maturation into active enzymes (22), so they have been used as targets for developing antivirals against SARS-CoV, Middle East respiratory syndrome CoV (MERS-CoV), and SARS-CoV-2 (23–25). The mature NSP12, a RNA-dependent RNA polymerase (RdRp), serves as the direct target of remdesivir (26) that was previously shown to inhibit SARS-CoV and MERS-CoV (27). Remdesivir antagonized SARS-CoV-2 viral replication with an EC_{50} of 0.7 μM (10) and exhibited marginal (68%) benefit in clinical trials on COVID-19 patients (28). Recently, a metallodrug, ranitidine bismuth citrate, was reported to suppress SARS-CoV-2 replication and relieve virus-associated pneumonia in Syrian hamsters by inhibiting the mature NSP13, a helicase (29).

$3CL^{pro}$ is chymotrypsin-like but utilizes the His-Cys dyad to cleave conserved sequences of (Leu,Met,Phe)-Gln↓(Ser,Ala,Gly) on the polyproteins of SARS-CoV (30). Several rationally designed peptidomimetics and FDA-approved or experimental drugs such as disulfiram, ebselen, tideglusib, TDZD-8, carmofur, and PX12 have been shown to inhibit $3CL^{pro}$ and SARS-CoV-2 replication (31–34). Moreover, boceprevir, GC-376, and calpain inhibitors II and XII have been demonstrated to inhibit SARS-CoV-2 viral replication by targeting $3CL^{pro}$ (11). As reported recently, the cysteine protease inhibitors MDL-28170 (calpain inhibitor III) and ONO 5334 (cathepsin K inhibitor) were found to antagonize SARS-CoV-2 viral replication (35). On the other hand, approved drugs as inhibitors of PL^{pro}, which can antagonize SARS-CoV-2 replication, have not been reported yet, although virtual screening studies have identified some candidate compounds (36). PL^{pro} is a Cys protease with an Asp-His-Cys triad for cleaving sequences of Leu-(Asn,Lys,Arg)-Gly-Gly↓(Ala,Lys). Recently, naphthalene-based inhibitors discovered previously (37) were shown to inhibit SARS-CoV-2 PL^{pro} activity and SARS-CoV-2 replication (38). More recently, two peptidomimetic inhibitors with α,β-unsaturated ester warhead toward the active site Cys of SARS-CoV-2 PL^{pro} were evaluated and their cocrystal structures with the proteases were solved to provide a framework for development of inhibitors with potential therapeutic value or drug repurposing (39).

To identify more marketed drugs with the potential to treat COVID-19 patients by targeting $3CL^{pro}$ and PL^{pro}, we established enzymatic assays for the proteases and characterized their kinetic constants and substrate specificities. We then performed a comprehensive screening on two large collections of drugs, one with 1,068 and the other with 2,701 FDA-approved drugs (the largest collection available so far). Using our $3CL^{pro}$ and PL^{pro} assays, we screened out 12 drugs as $3CL^{pro}$ inhibitors and 36 drugs as PL^{pro} inhibitors, respectively, which were active at 10 μM. By using plaque reduction assay, six drugs were shown to exhibit an EC_{50} below or close to 10 μM against the SARS-CoV-2 virus, and their antiviral mechanisms were investigated as reported herein.

RESULTS

Purification and characterization of $3CL^{pro}$ and PL^{pro}. $3CL^{pro}$ was expressed as a thioredoxin fusion protein with a His tag to facilitate its expression and purification as shown by reducing sodium dodecyl sulfate-polyacrylamide gel electrophoresis (SDS-

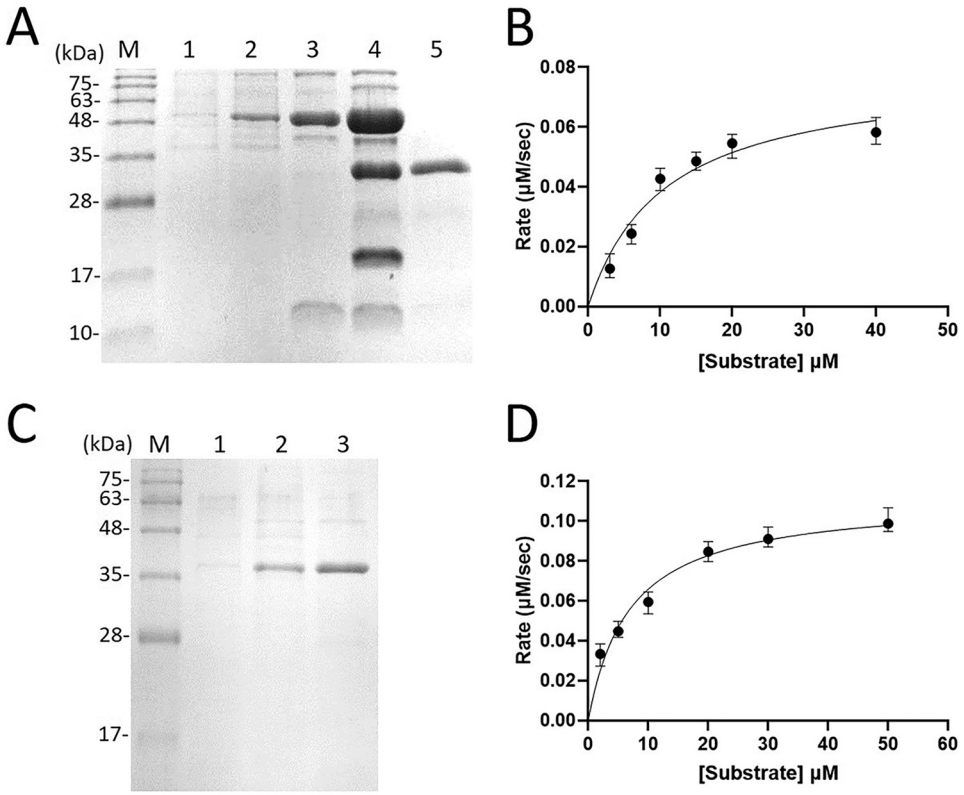

FIG 1 Preparation and characterization of SARS-CoV-2 3CL^{pro} and PL^{pro}. (A) SDS-PAGE analysis for the purification of the recombinant 3CL^{pro}. Lane M contains molecular mass markers of 100, 75, 63, 48, 35, 28, and 17 kDa. Lanes 1 and 2 show the cell lysate without and with IPTG induction to overexpress 3CL^{pro} fused with thioredoxin and His tag, respectively. Lane 3 is the tagged protease after Ni-NTA column chromatography. Lane 4 represents the tagged 3CL^{pro} treated with FXa to remove thioredoxin and His tag. Two extra bands, intact 3CL^{pro} and the thioredoxin-His tag with lower molecular mass, appear in this lane. Lane 5 shows the purified tag-free 3CL^{pro} after the Ni-NTA column. (B) Kinetic constants of 3CL^{pro}. The reaction initial rates of the protease were plotted against different substrate concentrations to yield the V_{max} and K_m values. (C) SDS-PAGE analysis for purifying the recombinant PL^{pro}. Lane M contains the molecular mass markers of 100, 75, 63, 48, 35, 28, and 17 kDa. Lanes 1 and 2 show the cell lysates without and with IPTG induction to overexpress PL^{pro} fused with thioredoxin and His tag, respectively. Lane 3 is the tagged PL^{pro} after Ni-NTA column chromatography. (D) Kinetic constants of PL^{pro}. The reaction initial rates of PL^{pro} were plotted against different substrate concentrations to yield the V_{max} and K_m values.

PAGE) (Fig. 1A). Using the fluorogenic peptide Dabcyl-KTSAVLQSGFRKME-Edans containing a fluorescence quenching pair as the substrate, the K_m value was determined to be $10.5 \pm 3.2\,\mu$M and the k_{cat} value was $2.2 \pm 0.3\ s^{-1}$ (Fig. 1B). The k_{cat}/K_m of SARS-CoV-2 3CL^{pro} with this fluorogenic substrate was $0.21\,\mu M^{-1}\ s^{-1}$, twofold higher than that ($0.11\,\mu M^{-1}\ s^{-1}$) for SARS-CoV 3CL^{pro} using the same substrate (40).

PL^{pro} was expressed with an N-terminal His tag to facilitate its purification using nickel-nitrilotriacetic acid (Ni-NTA) column as shown by the reducing SDS-PAGE (Fig. 1C). Using the commercially available fluorogenic peptide substrate Z-Arg-Leu-Arg-Gly-Gly-AMC, the K_m value was measured to be $6.9 \pm 1.4\,\mu$M and the k_{cat} value was $0.11 \pm 0.03\ s^{-1}$ (Fig. 1D). The catalytic efficiency k_{cat}/K_m of $0.016\,\mu M^{-1}\ s^{-1}$ is threefold higher than the $0.005\,\mu M^{-1}\ s^{-1}$ previously reported for SARS-CoV PL^{pro} using the same substrate (41). The purified recombinant 3CL^{pro} and PL^{pro} were used to screen FDA-approved drugs to find their inhibitors as shown below.

Substrate specificities of 3CL^{pro} and PL^{pro} were then examined using the 12-amino-acid (aa) peptides derived from their cleavage sequences on the polyproteins. The sequences of the 11 and 3 cleavage sites of the 3CL^{pro} and PL^{pro} are shown in Fig. 2A. When the 11 peptides were used as the substrates, the rates of their cleavage by 3CL^{pro} based on the high-performance liquid chromatography (HPLC) assay to monitor

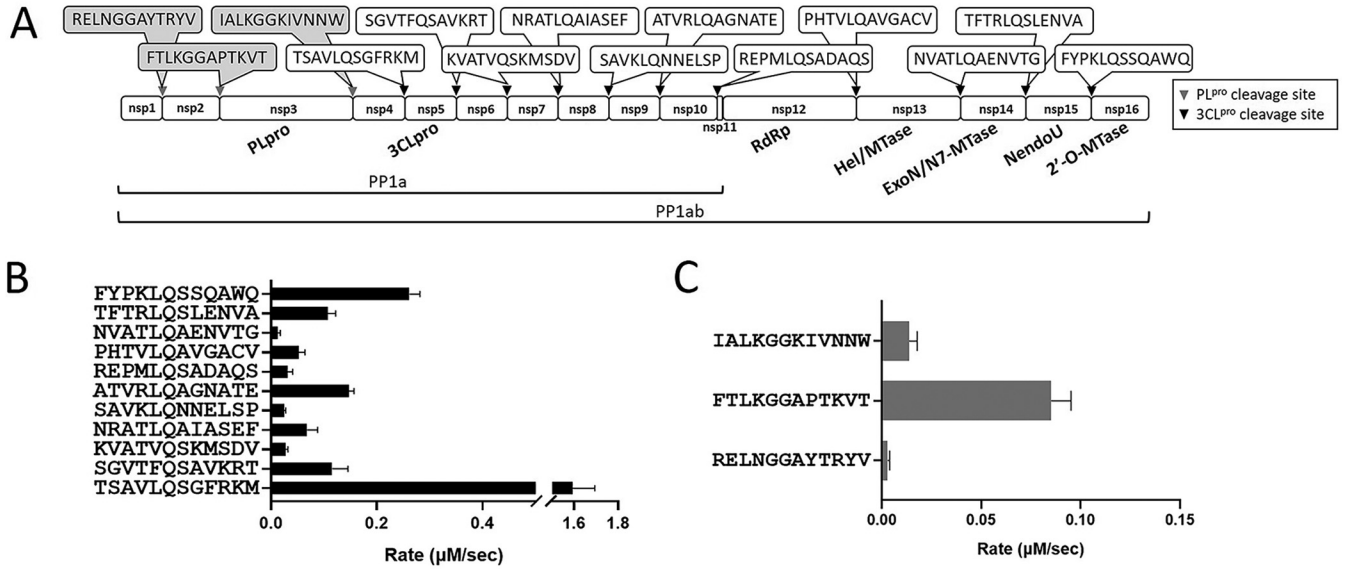

FIG 2 Substrate specificities of SARS CoV-2 3CL^{pro} and PL^{pro}. (A) On the PP1ab containing 16 nonstructural proteins (NSPs), the boxed sequences in gray and black represent the cleavage sites of PL^{pro} and 3CL^{pro}, respectively. Each synthetic peptide harbors 12 residues of each cleavage site. (B and C) Peptide cleavage rates by 3CL^{pro} (B) and PL^{pro} (C).

the formation of two fragments from 100 μM each peptide and 0.75 μM 3CL^{pro} at pH 7.0 are displayed in Fig. 2B and summarized in Table 1. The highest rate is 1.6 μM/s, obtained from the peptide of the N-terminal cleavage site. This is also the sequence used in the fluorescence resonance energy transfer (FRET) peptide substrate for assaying the 3CL^{pro} kinetics. The cleavage rates using 100 μM concentration of the three peptides as the substrates of 0.75 μM PL^{pro} are shown in Fig. 2C and summarized in Table 1. PL^{pro} cleaved its own N-terminal cleavage site most efficiently at a rate of 0.09 μM/s, its own C-terminal site at 0.01 μM/s, while that of the site between NSP1 and NSP2 at 0.003 μM/s was the lowest.

Screening of 1,068 and 2,701 FDA-approved drugs to find inhibitors of SARS-CoV-2 3CL^{pro}. After screening the 1,068 FDA-approved drugs by using the FRET assay, the compounds that inhibited 3CL^{pro} are colored in yellow and that inhibited both 3CL^{pro} and PL^{pro} are colored in green (please see Data Set S1 in the supplemental material). After excluding the highly toxic externally used drugs, we found one drug, tolcapone, that could inhibit 3CL^{pro} with a 50% inhibitory concentration (IC_{50}) of 7.9 μM (see Table S1 in the supplemental material and Fig. 3A). However, tolcapone showed a weak antiviral activity only at 50 μM (figure not shown).

The 2,701 FDA-approved drugs were screened against 3CL^{pro} and the compounds that inhibited 3CL^{pro} are colored in yellow and the compounds inhibited both 3CL^{pro} and PL^{pro} are colored in green (Data Set S2). After excluding the externally used medicines, 11 hits (Table S2) were identified as active in inhibiting 3CL^{pro} at 10 μM. Of these hits, only levothyroxine and manidipine-2HCl in addition to the previously reported 3CL^{pro} inhibitors were shown to inhibit virus replication by plaque reduction assay (see below). Here, the dose-dependent 3CL^{pro} inhibition curves were used to determine the IC_{50} values of levothyroxine and manidipine-2HCl being 19.2 $\pm$ 1.2 and 10.4 $\pm$ 1.6 μM, respectively (Fig. 3B and C).

Screening on 1,068 and 2,701 FDA-approved drugs to find inhibitors of SARS-CoV-2 PL^{pro}. Through screening the 1,068 FDA-approved drugs, we found 10 hits (Table S3) that could inhibit PL^{pro} activity when 10 μM was used in the assay. All the drugs screened are listed in Data Set S1, and the compounds that inhibited PL^{pro} are colored in blue and those inhibited both 3CL^{pro} and PL^{pro} are colored in green. However, only two drugs, maprotiline and reserpine, showed antiviral activity in the plaque reduction assay as shown later. The dose-dependent inhibition curves of

TABLE 1 Cleavage rates of the peptides by SARS-CoV-2 3CL^{pro} and PL^{pro}

Protease	Peptide	Cleavage rate (μM/s)
SARS-CoV-2 3CL^{pro}	TSAVLQSGFRKM	1.60 ± 0.12
	SGVTFQSAVKRT	0.12 ± 0.03
	KVATVQSKMSDV	0.03 ± 0.005
	NRATLQAIASEF	0.07 ± 0.02
	SAVKLQNNELSP	0.02 ± 0.003
	ATVRLQAGNATE	0.15 ± 0.011
	REPMLQSADAQS	0.03 ± 0.01
	PHTVLQAVGACV	0.05 ± 0.012
	NVATLQAENVTG	0.01 ± 0.005
	TFTRLQSLENVA	0.11 ± 0.015
	FYPKLQSSQAWQ	0.26 ± 0.02
SARS-CoV-2 PL^{pro}	RELNGGAYTRYV	0.003 ± 0.001
	FTLKGGAPTKVT	0.09 ± 0.012
	IALKGGKIVNNW	0.01 ± 0.004

maprotiline and reserpine were determined as shown in Fig. 4A and B, and the derived IC_{50} values were 9.7 ± 0.3 and 5.7 ± 0.7 μM, respectively.

Then 2,701 FDA-approved drugs were screened against PL^{pro} and 26 additional hits (Table S4) were identified. All the 2,701 drugs screened are listed in Data Set S2, and the compounds that inhibited PL^{pro} are colored in blue and those that inhibited both 3CL^{pro} and PL^{pro} are colored in green. Among these 26 hits, levothyroxine, loperamide, manidipine-2HCl, and proanthocyanidin were shown to inhibit virus replication by the plaque reduction assay as shown later. The dose-dependent inhibition curves of these four drugs were determined (Fig. 4C to F). Based on the data, the IC_{50} values for levothyroxine, loperamide, manidipine-2HCl, and proanthocyanidin were 15.3 ± 4.2, 33.5 ± 5.8, 14.2 ± 1.7, and 2.4 ± 0.3 μM, respectively.

Antiviral EC_{50} measurements of the inhibitors. As mentioned above, a total of 46 drugs from the two drug collections were identified as either 3CL^{pro} or PL^{pro} inhibitors and 2 drugs inhibited both at the concentration of 10 μM. The antiviral activities of these 46 drugs (10 μM) were tested using plaque reduction assay, and the active com-

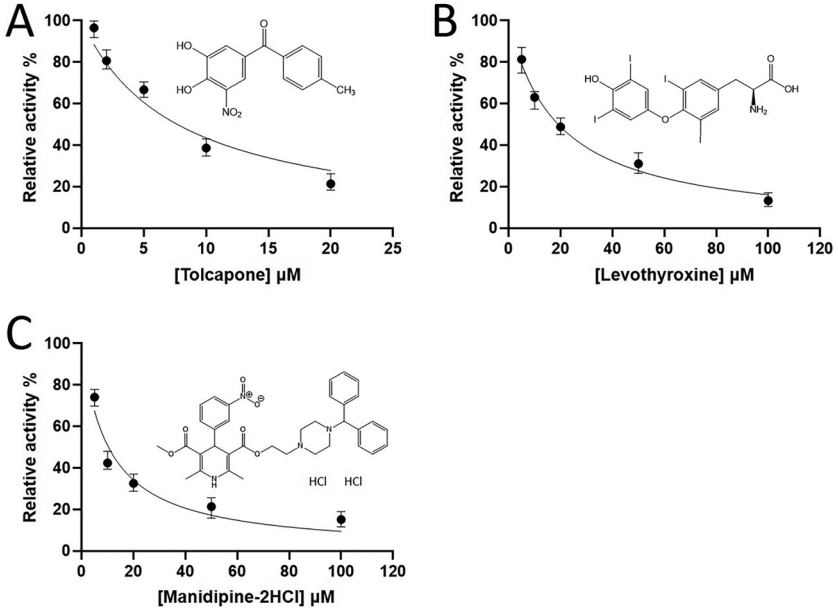

FIG 3 Screening and IC_{50} measurements of the 3CL^{pro} inhibitors. (A to C) The IC_{50} values of FDA-approved drugs, tolcapone, levothyroxine, and manidipine-2HCl, were measured to be 7.9 ± 0.9, 19.2 ± 1.2, and 10.4 ± 1.6, respectively, based on the inhibitor concentration-dependent curves.

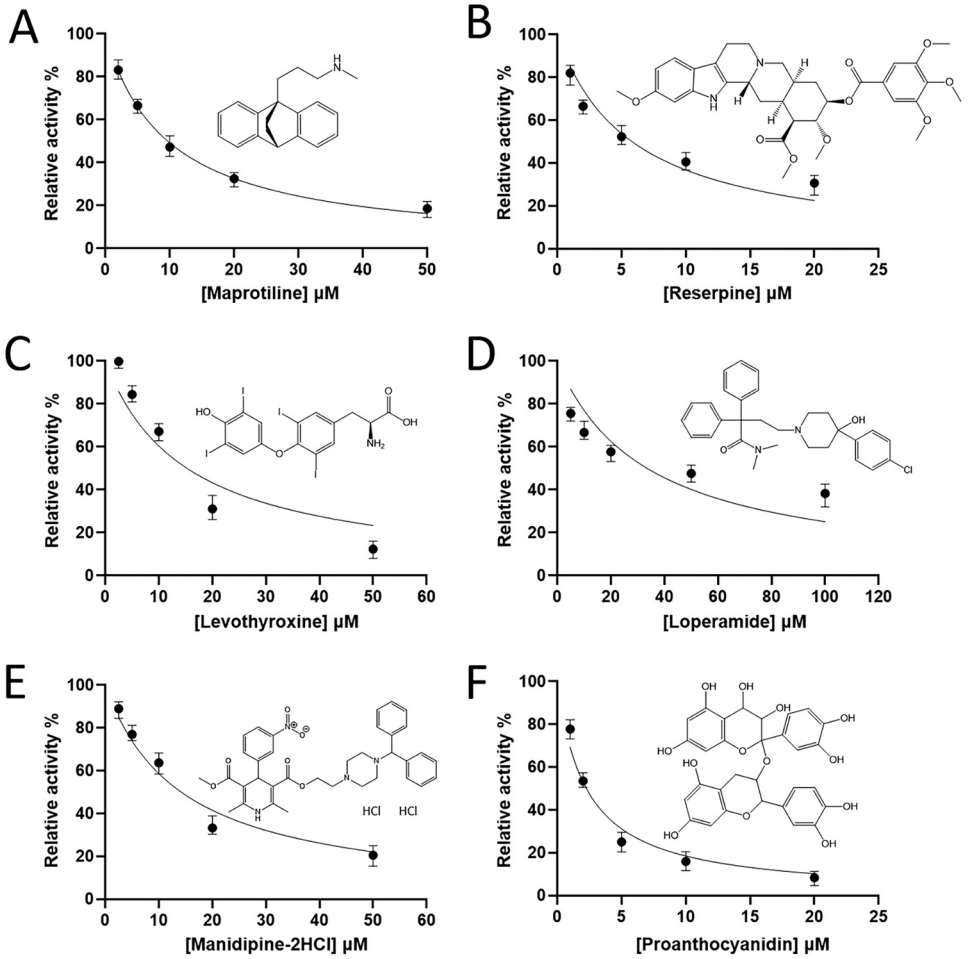

FIG 4 Screening and IC_{50} measurements of the PL^{pro} inhibitors. (A to D) FDA-approved drugs, maprotiline, reserpine, levothyroxine, loperamide, manidipine-2HCl, and proanthocyanidin were screened and found to be PL^{pro} inhibitors with IC_{50}s of 9.7 ± 0.3, 5.7 ± 0.7, 15.3 ± 4.2, 33.5 ± 5.8, 14.2 ± 1.7, and $2.4 \pm 0.3\ \mu$M, respectively, based on the inhibitor concentration-dependent curves.

pounds are colored red in supplemental tables. Initially, to maximize the chances to identify antivirals, we pretreated the cells with each drug, added each drug during the virus infection and after virus removal. By this full-time treatment as shown in Fig. 5A, we identified two $3CL^{pro}$-inhibiting drugs, levothyroxine and manidipine-2HCl, as well as six PL^{pro}-inhibiting drugs, levothyroxine, loperamide, manidipine-2HCl, maprotiline, reserpine, and proanthocyanidin, effective in reducing viral plaques. Next, two other treatment methods were performed to distinguish the stages for the drugs against SARS-CoV-2. As shown in Fig. 5A, "entry" was to pretreat the cells and virus during infection with each drug but without adding the drug after removal of virus, and "postentry" means each drug was added to the cells only after virus infection. By using these treatment methods, we suspected loperamide, manidipine-2HCl, and maprotiline antagonized viral replication by mainly inhibiting the viral protease(s) because postentry treatment could still inhibit the virus. In contrast, levothyroxine and proanthocyanidin suppressed the viral plaques probably by blocking the virus entry because postentry treatment could not inhibit the virus. Therefore, the measurements of EC_{50} were performed with "postentry" treatment for loperamide, manidipine-2HCl, and maprotiline and "entry" treatment for levothyroxine and proanthocyanidin as shown in Fig. 5A. For reserpine, apparent antiviral activity was observed only when full-time treatment was applied, and the EC_{50} was measured using full-time treatment (entry plus

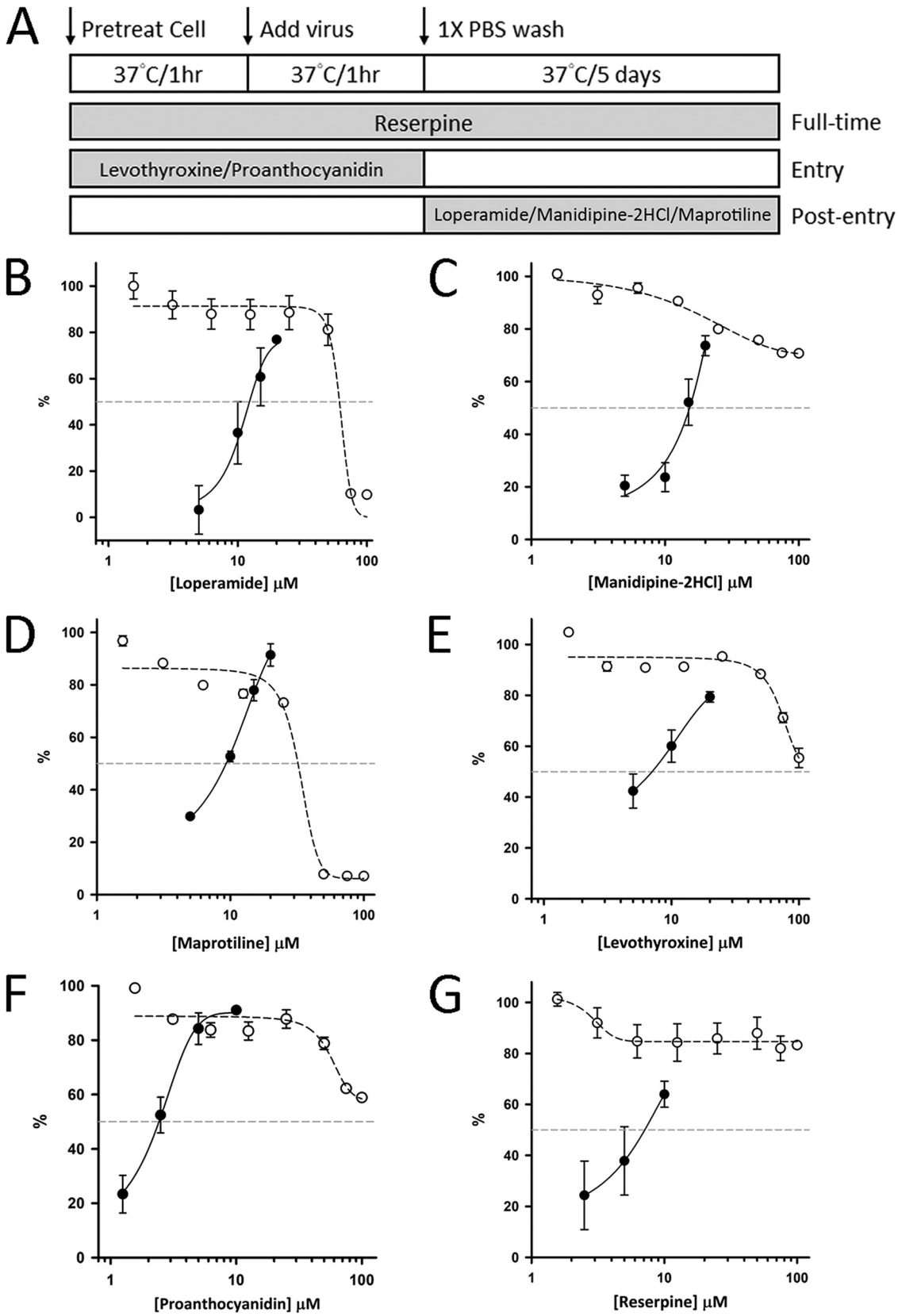

FIG 5 EC_{50} measurements of $3CL^{pro}$ and PL^{pro} inhibitors based on the plaque reduction assay. (A) Schematic illustration of the full-time, entry, and postentry experiments delineates the stage where the test drugs were added. (B to G) Six drugs identified from 1,068 and 2,701 drug collections showed apparent antiviral activity against the SARS-CoV-2 virus with EC_{50}s of 11.4 ± 1.6, 14.5 ± 0.8,

(Continued on next page)

postentry). The EC_{50} values for these drugs were determined accordingly using plaque reduction assay (see Fig. S1 in the supplemental material), and the plots of concentration-dependent virus plaque reduction under serially diluted drug concentrations are shown in Fig. 5B to G. The derived EC_{50} values for loperamide, manidipine-2HCl, maprotiline, levothyroxine, proanthocyanidin, and reserpine were 11.4 ± 1.6, 14.5 ± 0.8, 9.3 ± 0.1, 7.0 ± 2.2, 2.5 ± 0.4, and $6.6 \pm 1.5\ \mu$M, respectively. The 50% cytotoxic concentration (CC_{50}) values for loperamide and maprotiline were 56.4 ± 0.7 and $31.8 \pm 0.4\ \mu$M, respectively, and those for other drugs were all $>100\ \mu$M. The derived selectivity index (SI) for reserpine (SI $>$ 15.2), levothyroxine (SI $>$ 14.3), and proanthocyanidin (SI $>$ 40) were higher than 10, while those for loperamide (SI = 4.9), manidipine-2HCl (SI $>$ 6.9), and maprotiline (SI = 3.4) were below 10.

DISCUSSION

As demonstrated here, we have purified the recombinant $3CL^{pro}$ and PL^{pro} and monitored their activities using the fluorogenic peptide substrates (Fig. 1A to D). The kinetic efficiencies (k_{cat}/K_m) of two SARS-CoV-2 proteases are higher than that of SARS-CoV proteases. The cleavage rates of the examined peptides derived from their respective cleavage site sequences reveal that the N-terminal autocleavage reactions are the fastest for both $3CL^{pro}$ and PL^{pro} (Fig. 2A to C). This is probably due to the fact that the maturation of NSPs in two polyproteins requires first cleavage of the proteases' N termini. After cleavage of their N termini, the proteases become more flexible to undergo C-terminal cleavage toward fully active $3CL^{pro}$ and PL^{pro} which subsequently cleave other sites on the polyproteins. Our data also reveal the most preferred recognition sequences of Leu(P2)-Gln(P1)↓Ser(P1′) and Lys(P3)-Gly(P2)-Gly(P1)↓Ala(P1′) for SARS-CoV-2 $3CL^{pro}$ and PL^{pro}, respectively.

Using these assay platforms, we have screened the collections of 1,068 and 2,701 FDA-approved drugs and found 1 hit from 1,068 drugs and additional 11 hits from 2,701 drugs, which were active at 10 μM against $3CL^{pro}$. Of the hits, three drugs, disulfiram, ebselen, and boceprevir, have been previously reported (11, 33), and one drug, tolcapone, was previously found active in inhibiting feline CoV (42). Moreover, 10 hits from 1,068 drugs and additional 26 hits from 2,701 drugs, which displayed PL^{pro}-inhibiting activity at 10 μM were obtained from the screening. The inhibition concentration-dependent curves against the $3CL^{pro}$ (Fig. 3) and PL^{pro} (Fig. 4) for those drugs showing antiviral activities were determined. Note that although levothyroxine and manidipine-2HCl inhibit both $3CL^{pro}$ and PL^{pro} in the *in vitro* assay, their antiviral mechanisms vary. For example, levothyroxine exerts its antiviral activities at the entry step (EC_{50}=$7.0 \pm 2.2\ \mu$M) (Fig. 5E) instead of the postentry stage (EC_{50}>20 μM), while manidipine-2HCl exerts its antiviral activities only at the postentry stage (EC_{50}=$14.5 \pm 0.8\ \mu$M) (Fig. 5C). Interestingly, of the three PL^{pro} inhibitors showing anti-SARS-CoV-2 activities, proanthocyanidin, like levothyroxine, also showed strong antiviral activity at the entry step with the EC_{50} value of $2.5 \pm 0.4\ \mu$M (Fig. 5F). Therefore, levothyroxine and proanthocyanidin might block the entry of virus, which requires further experiments to prove. Another two PL^{pro}-only inhibitors, loperamide and maprotiline, showed antiviral activities at the postentry stage with the EC_{50} values of 11.4 ± 1.6 and $9.3 \pm 0.1\ \mu$M, respectively (Fig. 5B and D), but not the entry step, implying that they certainly inhibit virus replication inside the host cells. In contrast, reserpine exerts its antiviral activity only when it was given twice (entry plus postentry) (full time), suggesting that both its PL^{pro}-inhibiting and virus

FIG 5 Legend (Continued)
9.3 ± 0.1, 7.0 ± 2.2, 2.5 ± 0.4, and $6.6 \pm 1.5\ \mu$M for loperamide (B), manidipine-2HCl (C), maprotiline (D), levothyroxine (E), proanthocyanidin (F), and reserpine (G), respectively, as calculated from the dose-dependent plaque reduction percentages (see Fig. S1 in the supplemental material), represented by filled black circles. The sigmoidal fitting curves are shown with solid lines. The CC_{50} values for loperamide (B) and maprotiline (D) were 56.4 ± 0.7 and $31.8 \pm 0.4\ \mu$M, respectively, while those for other drugs were $>100\ \mu$M, based on the cell viability inhibition percentages, represented by open circles. The fitting curves are shown with dotted lines.

entry-inhibiting activities might contribute to its antivirus effect (EC_{50} = 6.6 ± 1.5 μM) (Fig. 5G). Therefore, the use of full-time, entry, and postentry treatments allows determination of the stages where the antiviral drugs exert their inhibitory effects.

Loperamide, sold under the brand name of Imodium, is a medication used to decrease the frequency of diarrhea. It is an opioid receptor agonist and acts on the μ-opioid receptors in the myenteric plexus of the large intestine to decrease the tone of the longitudinal and circular smooth muscles of the intestinal wall (43), thereby allowing more water to be absorbed from the fecal matter. Manidipine-2HCl is a calcium channel blocker (dihydropyridine type) that is used clinically as an antihypertensive (44). Maprotiline, sold under the brand name Ludiomil, is a tetracyclic antidepressant that is used in the treatment of depression. It is known to function as a norepinephrine reuptake inhibitor and also a strong antagonist of the H1 receptor (45). Reserpine is one of dozens of indole alkaloids isolated from the plant *Rauvolfia serpentine*. It is used for the treatment of high blood pressure by irreversibly blocking the H^+-coupled vesicular monoamine transporters, VMAT1 and VMAT2. It is the blockade of neuronal VMAT2 by reserpine that inhibits uptake and reduces stores of the monoamine neurotransmitters norepinephrine, dopamine, serotonin, and histamine in the synaptic vesicles of neurons (46). Reserpine was identified by our previous study (47) to inhibit SARS-CoV replication, but the target was not known until now to be PL^{pro} and virus entry. Its EC_{50} values against SARS-CoV was measured to be 3.4 μM (47). Six natural derivatives of reserpine were previously shown to exhibit activities toward SARS-CoV at less than 100 μM (47), and their activities against SARS-CoV-2 could be further examined in the future. Levothyroxine, also known as L-thyroxine, is a manufactured form of the thyroid hormone thyroxine (T4), used to treat thyroid hormone deficiency, including the severe form known as myxedema coma (48). Proanthocyanidins, a class of polyphenols found in a variety of plants, can function as antioxidants to remove harmful free oxygen radicals from cells. Therefore, proanthocyanidins have been known to confer significant health benefits as reported by several studies using human and animal models (49).

In summary, by using the $3CL^{pro}$ and PL^{pro} fluorescence assays, we identify six FDA-approved drugs which could suppress SARS-CoV-2. Considering the frequent uptake of loperamide and proanthocyanidins in some populations, it will be interesting to know the effectiveness of these drugs in prophylactic prevention of SARS-CoV-2 infection. We thus provide here candidates for prevention and/or treatment of COVID-19.

MATERIALS AND METHODS

Materials. Fluorogenic peptide substrate Dabcyl-KTSAVLQSGFRKME-Edans of $3CL^{pro}$ was synthesized by Yuan Yu Ltd. (Taiwan). The fluorogenic substrate peptide (Z-Arg-Leu-Arg-Gly-Gly-AMC) for PL^{pro} was purchased from Bachem (Bubendorf, Switzerland). The collections of 1,068 and 2,701 FDA-approved drugs were purchased from Target Molecule Corp. (Boston, MA, USA) and Selleck Chemicals (Houston, TX, USA), respectively. After screening, the active compounds in bulk size (e.g., 25 mg) were purchased from the companies for IC_{50}, EC_{50}, and CC_{50} measurements. The plasmid miniprep kit, DNA gel extraction kit, and Ni-NTA resin were purchased from Qiagen (Hilden, Germany). FXa and the protein expression kit, including pET32a and pET16b vectors as well as competent *Escherichia coli* JM109 and BL21(DE3) cells were obtained from Novagen (Merck KGaA, Darmstadt, Germany). The SARS-CoV-2 virus used in this study was SARS-CoV-2/NTU13/TWN/human/2020 (accession identifier [ID] EPI_ISL_422415) as previously described (50). All commercial buffers and reagents were of the highest grade.

Expression and purification of SARS-CoV-2 $3CL^{pro}$. The gene encoding SARS-CoV-2 $3CL^{pro}$ was synthesized by Genewiz Co. (South Plainfield, NJ, USA) and cloned into the pET32a vector by using PCR with the forward primer 5′-CAT GCC ATG GCT ATC GAG GGA AGG AGT GGT TTT AGG AAA ATG GC-3′ containing FXa and NcoI cleavage sequences and the reverse primer 5′-CCG CTC GAG TTA TTG GAA GGT AAC ACC AGA G-3′ containing XhoI site sequence (the underlined sequences encode the N and C termini of $3CL^{pro}$, respectively). The vector pET32a also encodes thioredoxin and His tag at the N terminus of the target protein. The recombinant $3CL^{pro}$ plasmid was then used to transform the *E. coli* JM109 competent cells and the transformed cells were streaked on a Luria-Bertani (LB) agar plate containing 100 μg/ml ampicillin. Ampicillin-resistant colonies were selected from the agar plate and sequenced to detect the *$3CL^{pro}$* gene. The correct construct was subsequently transformed to *E. coli* BL21(DE3) for protein expression. The 5-ml overnight culture of a single transformant was used to inoculate 500 ml of fresh LB medium containing 100 μg/ml ampicillin. The cells were grown to an optical density at 600 nm

(OD_{600}) of 0.6 and induced with 1 mM isopropyl-β-thiogalactopyranoside. After 4 to 5 h, the cells were harvested by centrifugation at 7,000 $\times$ *g* for 15 min.

The $3CL^{pro}$ purification was conducted at 4°C. The cell paste obtained from 1-liter cell culture was suspended in 40 ml lysis buffer containing 25 mM Tris-HCl (pH 7.5) and 150 mM NaCl. A French press instrument (AIM-AMINCO spectronic instruments; Cambridge Scientific Products, MA, USA) was used to disrupt the cells at 12,000 lb/in^2. The lysis solution was centrifuged, and the debris was discarded. The cell extract was loaded onto a 10-ml Ni-NTA column equilibrated with the same buffer containing 5 mM imidazole. The column was washed with 5 mM imidazole followed by 30 mM imidazole-containing buffer. The His-tagged $3CL^{pro}$ was eluted with the buffer containing 300 mM imidazole. The protein solution was dialyzed against 1 liter of lysis buffer two times. After overnight dialysis, the tagged $3CL^{pro}$ was treated with FXa protease to remove thioredoxin and His tag, and the mixture was loaded onto a Ni-NTA column equilibrated with the buffer containing 5 mM imidazole. The tag-free $3CL^{pro}$ in flowthrough was dialyzed against the buffer without imidazole (12 mM Tris-HCl [pH 7.5], 120 mM NaCl, 0.1 mM EDTA, and 2 mM dithiothreitol [DTT]) and stored at −70°C. The enzyme concentrations used in experiments were determined based on the absorbance at 280 nm.

Expression and purification of SARS-CoV-2 PL^{pro}. The gene encoding SARS-CoV-2 PL^{pro} was synthesized by Genewiz Co. (South Plainfield, NJ, USA) and cloned into the pET16b vector by using PCR with the forward primer 5′-CAT GCC ATG GCC CAT CAT CAT GAA GTG AGG ACT ATT AAG GTG-3′ containing NcoI cleavage sequence and reverse primer 5′-CCG CTC GAG TTA TAT GGT TGT GTA ACT GTT TTC TTT GTA G-3′ containing XhoI site sequence (the underlined sequences encode the N and C termini of PL^{pro}, respectively). The forward primer also encodes extra MAHHHHHH at the N terminus of the target protein. The recombinant PL^{pro} plasmid was then used to transform *E. coli* JM109 competent cells, and the transformed cells were streaked on a Luria-Bertani (LB) agar plate containing 100 μg/ml ampicillin. Ampicillin-resistant colonies were selected from the agar plate and sequenced for the *PL^{pro}* gene. The correct construct was subsequently transformed to *E. coli* BL21(DE3) for protein expression. The 5-ml overnight culture of a single transformant was used to inoculate 500 ml of fresh LB medium containing 100 μg/ml ampicillin. The cells were grown to an OD_{600} of 0.6 and induced with 1 mM isopropyl-β-thiogalactopyranoside. After 4 to 5 h, the cells were harvested by centrifugation at 7,000 $\times$ *g* for 15 min.

The PL^{pro} purification was conducted at 4°C. The cell paste obtained from 1-liter cell culture was suspended in 40 ml lysis buffer containing 25 mM Tris-HCl (pH 7.5) and 150 mM NaCl. A French press instrument (AIM-AMINCO spectronic instruments; Cambridge Scientific Products, MA, USA) was used to disrupt the cells at 12,000 lb/in^2. The lysis solution was centrifuged, and the debris was discarded. The cell extract was loaded onto a 10-ml Ni-NTA column equilibrated with the same buffer containing 5 mM imidazole. The column was washed with 5 mM imidazole followed by 30 mM imidazole-containing buffer. The His-tagged PL^{pro} was eluted with the buffer containing 300 mM imidazole. The His-tagged PL^{pro} in flowthrough was dialyzed into a buffer containing 12 mM Tris-HCl (pH 7.5), 120 mM NaCl, 0.1 mM EDTA, and 2 mM DTT for storage at −70°C. The enzyme concentrations used in all experiments were determined from the absorbance at 280 nm.

Kinetics of $3CL^{pro}$ and PL^{pro} measured using the fluorogenic substrates. The kinetic measurements were performed in the buffer (20 mM Bis-Tris [pH 7.0]) at 25°C. Enhanced fluorescence due to cleavage of the fluorogenic substrate peptide (Dabcyl-KTSAVLQSGFRKME-Edans) for $3CL^{pro}$ or (Z-Arg-Leu-Arg-Gly-Gly-AMC) for PL^{pro} was monitored at 538 and 460 nm, respectively, with excitation at 355 nm using a fluorescence plate reader (Fluoroskan Ascent; ThermoLabsystems, Sweden). The enzyme concentrations used for measuring K_m and V_{max} values were 35 nM for $3CL^{pro}$ and 75 nM for PL^{pro}, and the substrate concentrations were from 0.5- to 5-fold K_m values. $3CL^{pro}$ substrate concentration was determined by using the extinction coefficients 5,438 $M^{-1}\,cm^{-1}$ at 336 nm (Edans) and 15,100 $M^{-1}\,cm^{-1}$ at 472 nm (Dabcyl). PL^{pro} substrate concentration was determined by using the extinction coefficient of 17,800 $M^{-1}\,cm^{-1}$ at 354 nm (AMC). The initial rates within 10% substrate consumption under different substrate concentrations were used to calculate the kinetic parameters by fitting with the Michaelis-Menten equation ($V = V_{max}[S]/K_m + [S]$ where S is substrate) using KaleidaGraph computer program. For each data point, the measurements were repeated three times to yield the average number and standard deviation.

Peptide substrate specificity measurements. Peptides for testing as the substrates were chemically synthesized by Mission Biotech (Taipei, Taiwan) with a solid-phase methodology based on the sequences of cleavage sites on viral polyproteins (Fig. 2A). Reaction mixtures (100 μl) contained 0.75 μM protease and 100 μM each peptide in the buffer of 20 mM Bis-Tris (pH 7.0) for $3CL^{pro}$ or the buffer of 20 mM HEPES (pH 7.0) for PL^{pro}. Following incubation at 37°C for 0, 2.5, 5, and 10 min, reactions were stopped by adding 5 μl trifluoroacetic acid and applied to a C_{18} reverse-phase HPLC column (250 $\times$ 4.6 mm; Hichrom, Berkshire, UK). The column was eluted at room temperature with a linear acetonitrile gradient in the presence of 0.1% (vol/vol) trifluoroacetic acid at a flow rate of 1.0 ml/min. The areas of the product peaks monitored at 214 nm were integrated to calculate the cleavage rate of each peptide substrate under the catalysis of $3CL^{pro}$ or PL^{pro}.

Inhibition assay. The collections of drugs at 10 μM were screened for inhibiting the proteases, and the active inhibitors were confirmed three times. Only the IC_{50} values of the inhibitors which showed antiviral activity were measured in reaction mixtures containing 2.5 nM $3CL^{pro}$ with 6 μM fluorogenic substrate in a buffer of 20 mM Bis-Tris (pH 7.0) or 75 nM PL^{pro} with 10 μM fluorogenic substrate in a buffer of 20 mM Bis-Tris (pH 7.5) in the presence and absence of various concentrations of the inhibitors. The fluorescence changes that resulted from the reactions were followed over time at 538 nm with excitation at 355 nm for $3CL^{pro}$ or at 460 nm with excitation at 355 nm for PL^{pro} using the fluorescence plate

reader. The initial velocities of the inhibited reactions were plotted against the different inhibitor concentrations to yield the IC_{50} value by fitting with the equation: $A(I) = A(0) \times\{1 - [I/(I + IC_{50})]\}$. In this equation, $A(I)$ is the enzyme activity with inhibitor concentration I, $A(0)$ is the enzyme activity without inhibitor, and I is the inhibitor concentration. For each data point, the measurements were repeated three times to yield the average number and standard deviation.

Cell-based assay. For the SARS-CoV-2 plaque reduction assay, Vero E6 cells were seeded to a 24-well culture plate in Dulbecco modified Eagle medium (DMEM) with 10% FBS and antibiotics 1 day before infection. VeroE6 cells were infected by SARS-CoV-2 virus (50 to 100 PFU) for 1 h at 37°C. After removal of virus inoculum, the cells were washed once with phosphate-buffered saline (PBS) and overlaid with 1 ml overlay medium containing 1% methylcellulose for 5 days at 37°C. After 5 days, the cells were fixed with 10% formalin overnight. After removal of overlay media, the cells were stained with 0.5% crystal violet, and the plaques were counted. The percentage of inhibition was calculated as $[1 - (V_D/V_C)] \times 100\%$, where V_D and V_C refer to the virus titer in the presence and absence of the inhibitors, respectively. The minimal concentrations of compounds required to reduce plaque numbers 50% (EC_{50}) were calculated by regression analysis of the dose-response curves generated from plaque assays. For each data point, the measurements were repeated three times to yield the average number and standard deviation. To determine the stages where the drugs exert its antiviral effects, the drugs can be added before infection, during infection, or after infection as shown in Fig. 5A.

Cytotoxicity of the inhibitors was determined by using the acid phosphatase (ACP) assay. Briefly, Vero E6 cells were seeded onto a 96-well culture plate at a concentration of 2×10^4 cells per well. The next day, medium was removed, and each well was washed once with PBS before adding DMEM containing 2% FBS and different concentrations of inhibitors. Next, DMEM containing 2 μg/ml tosylsulfonyl phenylalanyl chloromethyl ketone (TPCK)-trypsin was added. After 1 h of incubation at 37°C, medium was removed, and cells were washed by PBS. Then, DMEM containing 2% FBS and different concentrations of each compound were added. After 3 days of incubation at 37°C, medium was removed, and each well was washed once with PBS. Next, buffer containing 0.1 M sodium acetate (pH 5.0), 0.1% Triton X-100, and 5 mM *p*-nitrophenyl phosphate was added. After incubating at 37°C for 2 h, 1 N NaOH was added to stop the reaction. The absorbance was then determined by an enzyme-linked immunosorbent assay (ELISA) reader (VERSAmax; Molecular Devices, Sunnyvale, CA) at a wavelength of 405 nm. The percentage of cytotoxicity was calculated using the following formula: cytotoxicity (%) = $[1 - (At/As) \times 100]$, where At and As refer to the absorbance of a tested substance and solvent control, respectively. The 50% cytotoxicity concentration (CC_{50}) was defined as the concentration reducing cell viability 50%. For each data point, the measurements were repeated three times to yield the average number and standard deviation.

SUPPLEMENTAL MATERIAL

Supplemental material is available online only.

SUPPLEMENTAL FILE 1, PDF file, 0.9 MB.

SUPPLEMENTAL FILE 2, XLSX file, 0.1 MB.

SUPPLEMENTAL FILE 3, XLSX file, 0.1 MB.

ACKNOWLEDGMENTS

This work was supported by grants (MOST109-2327-B-002-009, MOST109-2745-B-001-001, MOST109-3114-Y-001-001, and MOST109-2327-B-007-002) from the Ministry of Science and Technology, Taiwan. We also thank the support from Academia Sinica.

We declare that we have no conflicts of interest.

C.-J.K. and P.-H.L. designed the research. C.-J.K., T.-L.C. H.-C.K., Y.-M.T., Y.-K.L., and M.-C.H. performed the research. C.-J.K. and S.-Y.C. analyzed the data. L.H.-C.W. provided the drug libraries. P.-H.L. wrote the paper.

REFERENCES

1. Zhu N, Zhang D, Wang W, Li X, Yang B, Song J, Zhao X, Huang B, Shi W, Lu R, Niu P, Zhan F, Ma X, Wang D, Xu W, Wu G, Gao GF, Tan W, China Novel Coronavirus Investigating and Research Team. 2020. A novel coronavirus from patients with pneumonia in China, 2019. N Engl J Med 382:727–733. https://doi.org/10.1056/NEJMoa2001017.
2. Huang C, Wang Y, Li X, Ren L, Zhao J, Hu Y, Zhang L, Fan G, Xu J, Gu X, Cheng Z, Yu T, Xia J, Wei Y, Wu W, Xie X, Yin W, Li H, Liu M, Xiao Y, Gao H, Guo L, Xie J, Wang G, Jiang R, Gao Z, Jin Q, Wang J, Cao B. 2020. Clinical features of patients infected with 2019 novel coronavirus in Wuhan, China. Lancet 395:497–506. https://doi.org/10.1016/S0140-6736(20)30183-5.
3. Peiris JS, Lai ST, Poon LL, Guan Y, Yam LY, Lim W, Nicholls J, Yee WK, Yan WW, Cheung MT, Cheng VC, Chan KH, Tsang DN, Yung RW, Ng TK, Yuen KY, SARS study group. 2003. Coronavirus as a possible cause of severe acute respiratory syndrome. Lancet 361:1319–1325. https://doi.org/10.1016/S0140-6736(03)13077-2.
4. Ksiazek TG, Erdman D, Goldsmith CS, Zaki SR, Peret T, Emery S, Tong S, Urbani C, Comer JA, Lim W, Rollin PE, Dowell SF, Ling AE, Humphrey CD, Shieh WJ, Guarner J, Paddock CD, Rota P, Fields B, DeRisi J, Yang JY, Cox N, Hughes JM, LeDuc JW, Bellini WJ, Anderson LJ, SARS Working Group. 2003. A novel coronavirus associated with severe acute respiratory syndrome. N Engl J Med 348:1953–1966. https://doi.org/10.1056/NEJMoa030781.
5. Zaki AM, van Boheemen S, Bestebroer TM, Osterhaus AD, Fouchier RA. 2012. Isolation of a novel coronavirus from a man with pneumonia in Saudi Arabia. N Engl J Med 367:1814–1820. https://doi.org/10.1056/NEJMoa1211721.
6. Butler D. 2012. Clusters of coronavirus cases put scientists on alert. Nature 492:166–167. https://doi.org/10.1038/492166a.

7. Furuta Y, Komeno T, Nakamura T. 2017. Favipiravir (T-705), a broad spectrum inhibitor of viral RNA polymerase. Proc Jpn Acad Ser B Phys Biol Sci 93:449–463. https://doi.org/10.2183/pjab.93.027.
8. Chu CM, Cheng VC, Hung IF, Wong MM, Chan KH, Chan KS, Kao RY, Poon LL, Wong CL, Guan Y, Peiris JS, Yuen KY, HKU/UCH SARS Study Group. 2004. Role of lopinavir/ritonavir in the treatment of SARS: initial virological and clinical findings. Thorax 59:252–256. https://doi.org/10.1136/thorax.2003.012658.
9. De Wilde AH, Jochmans D, Posthuma CC, Zevenhoven-Dobbe JC, Van Nieuwkoop S, Bestebroer TM, Hoogen BGVD, Neyts J, Snijder EJ. 2014. Screening of an FDA-approved compound library identifies four small-molecule inhibitors of Middle East respiratory syndrome coronavirus replication in cell culture. Antimicrob Agents Chemother 58:4875–4884. https://doi.org/10.1128/AAC.03011-14.
10. Wang M, Cao R, Zhang L, Yang X, Liu J, Xu M, Shi Z, Hu Z, Zhong W, Xiao G. 2020. Remdesivir and chloroquine effectively inhibit the recently emerged novel coronavirus (2019-nCoV) in vitro. Cell Res 30:269–271. https://doi.org/10.1038/s41422-020-0282-0.
11. Ma C, Sacco MD, Hurst B, Townsend JA, Hu Y, Szeto T, Zhang X, Tarbet B, Marty MT, Chen Y, Wang J. 2020. Boceprevir, GC-376, and calpain inhibitors II, XII inhibit SARS-CoV-2 viral replication by targeting the viral main protease. Cell Res 30:678–692. https://doi.org/10.1038/s41422-020-0356-z.
12. Savarino A, Boelaert JR, Cassone A, Majori G, Cauda R. 2003. Effects of chloroquine on viral infections: an old drug against today's diseases. Lancet Infect Dis 3:722–727. https://doi.org/10.1016/S1473-3099(03)00806-5.
13. González Canga A, Sahagún Prieto AM, Diez Liébana MJ, Fernández Martínez N, Sierra Vega M, García Vieitez JJ. 2008. The pharmacokinetics and interactions of ivermectin in humans–a mini-review. AAPS J 10:42–46. https://doi.org/10.1208/s12248-007-9000-9.
14. Wagstaff KM, Sivakumaran H, Heaton SM, Harrich D, Jans DA. 2012. Ivermectin is a specific inhibitor of importin alpha/beta-mediated nuclear import able to inhibit replication of HIV-1 and dengue virus. Biochem J 443:851–856. https://doi.org/10.1042/BJ20120150.
15. Kadam RU, Wilson IA. 2017. Structural basis of influenza virus fusion inhibition by the antiviral drug Arbidol. Proc Natl Acad Sci U S A 114:206–214. https://doi.org/10.1073/pnas.1617020114.
16. Caly L, Druce JD, Catton MG, Jans DA, Wagstaff KM. 2020. The FDA-approved drug Ivermectin inhibits the replication of SARS-CoV-2 in vitro. Antiviral Res 178:104787. https://doi.org/10.1016/j.antiviral.2020.104787.
17. Wang X, Cao R, Zhang H, Liu J, Xu M, Hu H, Li Y, Zhao L, Li W, Sun X, Yang X, Shi Z, Deng F, Hu Z, Zhong W, Wang M. 2020. The anti-influenza virus drug, arbidol is an efficient inhibitor of SARS-CoV-2 in vitro. Cell Discov 6:28. https://doi.org/10.1038/s41421-020-0169-8.
18. Hoffmann M, Mösbauer K, Hofmann-Winkler H, Kaul A, Kleine-Weber H, Krüger N, Gassen NC, Müller MA, Drosten C, Pöhlmann S. 2020. Chloroquine does not inhibit infection of human lung cells with SARS-CoV-2. Nature 585:588–590. https://doi.org/10.1038/s41586-020-2575-3.
19. Liu J, Cao R, Xu M, Wang X, Zhang H, Hu H, Li Y, Hu Z, Zhong W, Wang M. 2020. Hydroxychloroquine, a less toxic derivative of chloroquine, is effective in inhibiting SARS-CoV-2 infection in vitro. Cell Discov 6:16. https://doi.org/10.1038/s41421-020-0156-0.
20. Funnell SGP, Dowling WE, Muñoz-Fontela C, Gsell PS, Ingber DE, Hamilton GA, Delang L, Rocha-Pereira J, Kaptein S, Dallmeier KH, Neyts J, Rosenke K, de Wit E, Feldmann H, Maisonnasse P, Le Grand R, Frieman MB, Coleman CM. 2020. Emerging preclinical evidence does not support broad use of hydroxychloroquine in COVID-19 patients. Nat Commun 11:4253. https://doi.org/10.1038/s41467-020-17907-w.
21. Wu F, Zhao S, Yu B, Chen YM, Wang W, Song ZG, Hu Y, Tao ZW, Tian JH, Pei YY, Yuan ML, Zhang YL, Dai FH, Liu Y, Wang QM, Zheng JJ, Xu L, Holmes EC, Zhang YZ. 2020. A new coronavirus associated with human respiratory disease in China. Nature 579:265–269. https://doi.org/10.1038/s41586-020-2008-3.
22. Hsu MF, Kuo CJ, Chang KT, Chang HC, Chou CC, Ko TP, Shr HL, Chang GG, Wang AH, Liang PH. 2005. Mechanism of the maturation process of SARS-CoV 3CL protease. J Biol Chem 280:31257–31266. https://doi.org/10.1074/jbc.M502577200.
23. Pillaiyar T, Manickam M, Namasivayam V, Hayashi Y, Jung SH. 2016. An overview of Severe Acute Respiratory Syndrome-Coronavirus (SARS-CoV) 3CL protease inhibitors: peptidomimetics and small molecule chemotherapy. J Med Chem 59:6595–6628. https://doi.org/10.1021/acs.jmedchem.5b01461.
24. He J, Hu L, Huang X, Wang C, Zhang Z, Wang Y, Zhang D, Ye W. 2020. Potential of coronavirus 3C-like protease inhibitors for the development of new anti-SARS-CoV-2 drugs: insights from structures of protease and inhibitors. Int J Antimicrob Agents 56:106055. https://doi.org/10.1016/j.ijantimicag.2020.106055.
25. Báez-Santos YM, St John SE, Mesecar AD. 2015. The SARS-coronavirus papain-like protease: structure, function and inhibition by designed antiviral compounds. Antiviral Res 115:21–38. https://doi.org/10.1016/j.antiviral.2014.12.015.
26. Gordon CJ, Tchesnokov EP, Woolner E, Perry JK, Feng JY, Porter DP, Götte M. 2020. Remdesivir is a direct-acting antiviral that inhibits RNA-dependent RNA polymerase from Severe Acute Respiratory Syndrome Coronavirus 2 with high potency. J Biol Chem 295:6785–6797. https://doi.org/10.1074/jbc.RA120.013679.
27. Sheahan TP, Sims AC, Graham RL, Menachery VD, Gralinski LE, Case JB, Leist SR, Pyrc K, Feng JY, Trantcheva I, Bannister R, Park Y, Babusis D, Clarke MO, Mackman RL, Spahn JE, Palmiotti CA, Siegel D, Ray AS, Cihlar T, Jordan R, Denison MR, Baric RS. 2017. Broad-spectrum antiviral GS-5734 inhibits both epidemic and zoonotic coronaviruses. Sci Transl Med 9:eaal3653. https://doi.org/10.1126/scitranslmed.aal3653.
28. Grein J, Ohmagari N, Shin D, Diaz G, Asperges E, Castagna A, Feldt T, Green G, Green ML, Lescure FX, Nicastri E, Oda R, Yo K, Quiros-Roldan E, Studemeister A, Redinski J, Ahmed S, Bernett J, Chelliah D, Chen D, Chihara S, Cohen SH, Cunningham J, D'Arminio Monforte A, Ismail S, Kato H, Lapadula G, L'Her E, Maeno T, Majumder S, Massari M, Mora-Rillo M, Mutoh Y, Nguyen D, Verweij E, Zoufaly A, Osinusi AO, DeZure A, Zhao Y, Zhong L, Chokkalingam A, Elboudwarej E, Telep L, Timbs L, Henne I, Sellers S, Cao H, Tan SK, Winterbourne L, Desai P, Mera R, et alet al. 2020. Compassionate use of Remdesivir for patients with severe Covid-19. N Engl J Med 382:2327–2336. https://doi.org/10.1056/NEJMoa2007016.
29. Yuan S, Wang R, Chan JF, Zhang AJ, Cheng T, Chik KK, Ye ZW, Wang S, Lee AC, Jin L, Li H, Jin DY, Yuen KY, Sun H. 2020. Metallodrug ranitidine bismuth citrate suppresses SARS-CoV-2 replication and relieves virus-associated pneumonia in Syrian hamsters. Nat Microbiol 5:1439–1448. https://doi.org/10.1038/s41564-020-00802-x.
30. Chuck CP, Chong LT, Chen C, Chow HF, Wan DC, Wong KB. 2010. Profiling of substrate specificity of SARS-CoV 3CL. PLoS One 5:e13197. https://doi.org/10.1371/journal.pone.0013197.
31. Zhang L, Lin D, Sun X, Curth U, Drosten C, Sauerhering L, Becker S, Rox K, Hilgenfeld R. 2020. X-ray structure of main protease of the novel coronavirus SARS-CoV-2 enables design of α-hetoamide inhibitors. Science 368:409–412. https://doi.org/10.1126/science.abb3405.
32. Dai W, Zhang B, Jiang XM, Su H, Li J, Zhao Y, Xie X, Jin Z, Peng J, Liu F, Li C, Li Y, Bai F, Wang H, Cheng X, Cen X, Hu S, Yang X, Wang J, Liu X, Xiao G, Jiang H, Rao Z, Zhang LK, Xu Y, Yang H, Liu H. 2020. Structure-based design of antiviral drug candidates targeting SARS-CoV-2 main protease. Science 368:1331–1335. https://doi.org/10.1126/science.abb4489.
33. Jin Z, Du X, Xu Y, Deng Y, Liu M, Zhao Y, Zhang B, Li X, Zhang L, Peng C, Duan Y, Yu J, Wang L, Yang K, Liu F, Jiang R, Yang X, You T, Liu X, Yang X, Bai F, Liu H, Liu X, Guddat LW, Xu W, Xiao G, Qin C, Shi Z, Jiang H, Rao Z, Yang H. 2020. Structure of Mpro from COVID-19 virus and discovery of its inhibitors. Nature 582:289−293. https://doi.org/10.1038/s41586-020-2223-y.
34. Jin Z, Zhao Y, Sun Y, Zhang B, Wang H, Wu Y, Zhu Y, Zhu C, Hu T, Du X, Duan Y, Yu J, Yang X, Yang X, Yang K, Liu X, Guddat LW, Xiao G, Zhang L, Yang H, Rao Z. 2020. Structural basis for the inhibition of SARS-CoV-2 main protease by antineoplastic drug carmofur. Nat Struct Mol Biol 27:529–532. https://doi.org/10.1038/s41594-020-0440-6.
35. Riva L, Yuan S, Yin X, Martin-Sancho L, Matsunaga N, Pache L, Burgstaller-Muehlbacher S, De Jesus PD, Teriete P, Hull MV, Chang MW, Chan JF, Cao J, Poon VK, Herbert KM, Cheng K, Nguyen TH, Rubanov A, Pu Y, Nguyen C, Choi A, Rathnasinghe R, Schotsaert M, Miorin L, Dejosez M, Zwaka TP, Sit KY, Martinez-Sobrido L, Liu WC, White KM, Chapman ME, Lendy EK, Glynne RJ, Albrecht R, Ruppin E, Mesecar AD, Johnson JR, Benner C, Sun R, Schultz PG, Su AI, García-Sastre A, Chatterjee AK, Yuen KY, Chanda SK. 2020. Discovery of SARS-CoV-2 antiviral drugs through large-scale compound repurposing. Nature 586:113–119. https://doi.org/10.1038/s41586-020-2577-1.
36. Kandeel M, Abdelrahman AHM, Oh-Hashi K, Ibrahim A, Venugopala KN, Morsy MA, Ibrahim MAA. 2020. Repurposing of FDA-approved antivirals, antibiotics, anthelmintics, antioxidants, and cell protectives against SARS-CoV-2 papain-like protease. J Biomol Struct Dyn https://doi.org/10.1080/07391102.2020.1784291.
37. Ghosh AK, Takayama J, Aubin Y, Ratia K, Chaudhuri R, Baez Y, Sleeman K, Coughlin M, Nichols DB, Mulhearn DC, Prabhakar BS, Baker SC, Johnson ME, Mesecar AD. 2009. Structure-based design, synthesis, and biological

evaluation of a series of novel and reversible inhibitors for the Severe Acute Respiratory Syndrome-Coronavirus papain-like protease. J Med Chem 52:5228–5240. https://doi.org/10.1021/jm900611t.
38. Freitas BT, Durie IA, Murray J, Longo JE, Miller HC, Crich D, Hogan RJ, Tripp RA, Pegan SD. 2020. Characterization and noncovalent inhibition of the deubiquitinase and deISGylase activity of SARS-CoV-2 papain-like protease. ACS Infect Dis 6:2099–2109. https://doi.org/10.1021/acsinfecdis.0c00168.
39. Rut W, Lv Z, Zmudzinski M, Patchett S, Nayak D, Snipas SJ, Oualid FE, Huang TT, Bekes M, Drag M, Olsen SK. 2020. Activity profiling and crystal structures of inhibitor-bound SARS-CoV-2 papain-like protease: a framework for anti-COVID-19 drug design. Sci Adv 6:eabd4596. https://doi.org/10.1126/sciadv.abd4596.
40. Kuo CJ, Chi YH, Hsu JT, Liang PH. 2004. Characterization of SARS main protease and inhibitor assay using a fluorogenic substrate. Biochem Biophys Res Commun 318:862–867. https://doi.org/10.1016/j.bbrc.2004.04.098.
41. Chen Y, Savinov SN, Mielech AM, Cao T, Baker SC, Mesecar AD. 2015. X-ray structural and functional studies of the three tandemly linked domains of non-structural protein 3 (nsp3) from Murine Hepatitis Virus reveal conserved functions. J Biol Chem 290:25293–25306. https://doi.org/10.1074/jbc.M115.662130.
42. Ke YY, Peng TT, Yeh TK, Huang WZ, Chang SE, Wu SH, Hung HC, Hsu TA, Lee SJ, Song JS, Lin WH, Chiang TJ, Lin JH, Sytwu HK, Chen CT. 2020. Artificial intelligence approach fighting COVID-19 with repurposing drugs. Biomed J 43:355–362. https://doi.org/10.1016/j.bj.2020.05.001.
43. Hanauer SB. 2008. The role of loperamide in gastrointestinal disorders. Rev Gastro Disord 8:15–20.
44. Mizuno K, Haga H, Takahashi M, Fukuchi S. 1992. Evaluation of manidipine hydrochloride, a new calcium antagonist, in the treatment of hypertensive patients with renal disorders. Curr Ther Res 52:248–253. https://doi.org/10.1016/S0011-393X(05)80475-8.
45. Peng WH, Lo KL, Lee YH, Hung TH, Lin YC. 2007. Berberine produces antidepressant-like effects in the forced swim test and in the tail suspension test in mice. Life Sci 81:933–938. https://doi.org/10.1016/j.lfs.2007.08.003.
46. Yaffe D, Forrest LR, Schuldiner S. 2018. The ins and outs of vesicular monoamine transporters. J Gen Physiol 150:671–682. https://doi.org/10.1085/jgp.201711980.
47. Wu CY, Jan JT, Ma SH, Kuo CJ, Juan HF, Cheng YS, Hsu HH, Huang HC, Wu D, Brik A, Liang FS, Liu RS, Fang JM, Chen ST, Liang PH, Wong CH. 2004. Small molecules targeting severe acute respiratory syndrome human coronavirus. Proc Natl Acad Sci U S A 101:10012–10017. https://doi.org/10.1073/pnas.0403596101.
48. Mandel SJ, Brent GA, Larsen PR. 1993. Levothyroxine therapy in patients with thyroid disease. Ann Intern Med 119:492–502. https://doi.org/10.7326/0003-4819-119-6-199309150-00009.
49. Rauf A, Imran M, Abu-Izneid T, Iahtisham U-H, Patel S, Pan X, Naz S, Sanches Silva A, Saeed F, Rasul Suleria HA. 2019. Proanthocyanidins: a comprehensive review. Biomed Pharmacother 116:108999. https://doi.org/10.1016/j.biopha.2019.108999.
50. Huang KY, Lin MS, Kuo TC, Chen CL, Lin CC, Chou YC, Chao TL, Pang YH, Kao HC, Huang RS, Lin S, Chang SY, Yang PC. 2021. Humanized COVID-19 decoy antibody effectively blocks viral entry and prevents SARS-CoV-2 infection. EMBO Mol Med 13:e12828.